



# An Impedance Behavior Study of Commercial NCA Cylindrical Battery Cells at Different SOCs

Yuanyuan Xie, 1,\*,z Donghoon Kim, 2,\*,z Miyoung Lee, Inhyeong Park, and Woonki Na<sup>3,z</sup>

The impedance behavior of a commercial Nickel-cobalt-aluminum(NCA) cylindrical cell was studied in this work. A series of impedance experiments was designed to explore the impact of battery state of charge (SOC) and other operating conditions. Our results indicated the impedance response of this cylindrical battery varies with the state of charge in both charge and discharge process. Experimental results also showed the SOC dependent impedance existed in different operating temperatures and C-rates. An impedance model was developed to explore the potential mechanisms behind experimental observations. Model results showed that the operating temperature and charge-discharge rate could significantly influence the impedance response of the battery but could not directly cause the variation of the impedance response at different SOC conditions. Results also showed that the contact resistance variation, resulted from the expansion and contraction of cell electrodes during charge and discharge, could lead to a SOC dependent impedance behavior of the commercial cell and influence battery output performance.

© 2021 The Electrochemical Society ("ECS"). Published on behalf of ECS by IOP Publishing Limited. [DOI: 10.1149/1945-7111/ac2706]

Manuscript submitted July 25, 2021; revised manuscript received September 1, 2021. Published September 23, 2021.

The classic 18650 format cylindrical Li-ion battery has been widely used today by electric vehicles (EVs), which has a wound jelly-roll structure in a form of an Archimedean spiral. <sup>1,2</sup> Comparing to the stacked electrodes, such wound electrodes can be produced faster and provide a relatively higher energy density in the limited given space on the electric vehicles. <sup>3,4</sup> With the help of numerous research activities by battery makers, an optimized manufacturing procedure from the material selection through electrode production to cell fabrication and quality control has been well established, which gives these commercial cylindrical cells a stable structure and cycling performance.

The safety issues of Li-ion batteries have always attracted great interest today especially for EV on-board batteries, which are related to the charge and heat transport processes and are significantly influenced by battery cell geometry and configurations. The electrochemical impedance spectroscopy (EIS) is widely adopted as an effective technique for determining the electrochemical behavior and state of health of the batteries, 5,6 which is typically obtained through an active interrogation process: an alternating voltage perturbation is applied to excite the battery cell with frequencies ranging from very low to extremely high, while the corresponding battery current output is recorded and used to calculate the generalized battery resistance. The impedance spectra contain the fundamental information of battery internal reaction and transport procedures. If the battery EIS profiles under different operating conditions can be deconvoluted properly, it can not only provide insights into the battery degradation process to facilitate the high safety EV battery designs, but also benefit the EV battery management through understanding the fundamentals of battery behavior.

Although numerous EIS testing and measurements have been carried out to investigate the performance of commercial cylindrical Li-ion batteries, 7-10 the interpretation of EIS are typically using equivalent circuit method along with experimental investigation, which uses electrical circuits to simulate and predict battery generalized resistance. 11-13 The simplicity of the equivalent circuit method provides fast computations. However, without taking the physicochemical principles of lithium-ion batteries into consideration, the results obtained from equivalent circuit analysis cannot avoid information loss and has poor accuracy on parameter predictions under different battery operating conditions. 14 Hence, to understand the behavior of commercial cylindrical cell under different operating

In this study, we firstly designed and conducted EIS testing on commercial 18650 cylindrical cells and explored their behavior at different state of charge, temperature, and C-rate. Then, a mathematical model was developed by considering both transport processes and electrochemical reactions inside battery. Together with the experiments, we used our model to reproduce the experimental procedure and studied the influence of SOC, temperature and C-rate on battery impedance response, which eventually could reveal the mechanisms behind the experimental observations.

## **Experimental**

Experimental testing was carried out using six identical commercial 18650 lithium-ion battery cells provided by Samsung. In the battery cells, NCA electrode and graphite electrode were used as cell cathode and anode respectively, and the thickness of electrodes is around 120 um. The electrolyte is 1 M LiPF6 in EC/EMC and the separator layer applied is a Celgard product with a thickness of 6 um. Six well-cycled 18650 cells were placed in a temperature-controlled chamber for testing, which was set at 25 °C and was connected to a 16-channel galvanostat/potentiostat battery cycler (BioLogic Product). In the BT-Lab platform, the cutoff potentials were set to be 4.2 V (set as 100% SOC) and 2.5 V (set as 0%SOC), while the potential data were recorded every other second. Following the instruction provided by Samsung (rate limits of this type of cell), a discharge rate performance test was firstly conducted at 25 °C: 18650 cells were discharged from fully charged state to fully discharged state at 0.1C, 1C and 4C respectively, then a charge rate performance test was carried out at 0.1C and 1C, respectively, from fully discharged state to fully charged state (cell manual indicates that the charging rate should not exceed 1.6C). Then, a series of impedance measurement experiments was designed and carried out.

Our impedance testing protocols are as follows: the cylindrical cells were firstly fully charged to and maintained at 4.2 V for 30 min, then the cells were discharged at 0.1C. During this discharge process, a two-hours open circuit relaxation was applied and a EIS test (5 mV, 10mHz~10 kHz) was performed after every 30 min. In this way, the impedance behavior of these commercial cylindrical cells can be obtained every 10% depth of discharge (DOD). The same testing protocol was used at 1C and 4C constant discharging rates. During 1C and 4C testing, the EIS test was carried out after

<sup>&</sup>lt;sup>1</sup>Department of Mechanical Engineering, California State University, Fresno, California, United States of America

<sup>&</sup>lt;sup>2</sup>Department of Electrical Engineering, Chungnam National University, Daejeon, Korea

<sup>&</sup>lt;sup>3</sup> Department of Electrical and Computer Engineering, California State University, Fresno, California, United States of America

conditions, we designed a series of EIS experiments and developed an electrochemical model to analyze the related mechanisms behind the observed impedance responses.

<sup>\*</sup>Electrochemical Society Member.

<sup>&</sup>lt;sup>z</sup>E-mail: yxie@csufresno.edu; whdgns0422@cnu.ac.kr; wkna@mail.fresnostate.edu

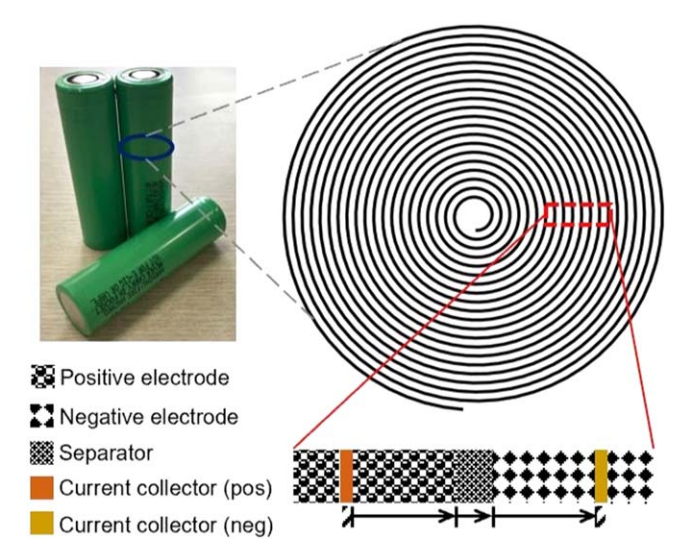


Figure 1. Cell structure and model geometry.

every 3 min and every 45 s respectively to make sure the impedance was measured at the same DOD. After discharge test, we further performed the charging procedure test. The charge testing protocol was similar to the discharging test but it was started from a fully discharge state at 2.5 V, and EIS testing was performed after every 5% depth of charge at 0.1C and 1C respectively. After this group of discharge and charge EIS testing, we changed the temperature of the temperature-controlled chamber from 25 °C to 10 °C and repeated above EIS testing experiments.

### Modeling

The commercial 18650 cell has a wound jelly-roll structure. As shown in Fig. 1, the cross section of the cell consists of positive NCA electrode, separator, negative graphite electrode and current collector layers, which are wound through a near Archimedean spiral locus, and their thickness can be assumed to be uniform based on Samsung's cell manufacturing procedure. Since the commercial electrodes are prepared by double side coating on the foil current collector, a symmetrical boundary can be assumed on both end surface of the current collector layer. The influences of cell anisotropic diffusion, structure, volume changes and other non-idealities are all neglected. Then, a porous electrode model can be developed: in the electrodes, the total current transferred between the

solid electrode particles and the electrolyte solution can be formulated as the sum of the Faradaic current and the electrical double layer current: <sup>15</sup>

$$i_j^{tot} = i_j^F + i_j^{dl}, j = neg, pos$$
 [1]

$$\begin{split} i_{j}^{F} &= i_{j}^{0} F S_{j} \Biggl\{ \exp \Biggl( \frac{z \alpha_{j}^{a} F}{R T} \eta_{j} \Biggr) - \exp \Biggl( - \frac{z \alpha_{j}^{a} F}{R T} \eta_{j} \Biggr) \Biggr\}, \\ i_{j}^{dl} &= C_{dl,j} S_{j} \frac{\partial}{\partial t} (\varphi_{1,j} - \varphi_{1,f}) \end{split} \tag{2}$$

where, j stands for negative electrode (neg) or positive electrode (pos);  $i_i^0$  is the exchange current density;  $S_i$  is the specific interfacial area;  $C_{dl,j}$  is the electrical double layer capacity;  $\eta_j$  is the overpotential;  $\varphi_{1,f}$  is the potential in the SEI  $\varphi_{1,f} = \varphi_{2,j} + (i_j^F + i_j^{dl})R_f$ ;  $\varphi_{1,j}$  and  $\varphi_{2,j}$  are the potentials in solid phase and liquid phase respectively. All side reaction currents (e.g., current of SEI film formation, etc.) are neglected here given the fact that the reported capacity retention of most commercial 18650 cells could be 95% after 400 cycles of charge and discharge operation. 16 The governing equations of charge, mass and heat transfer processes in both solid electrode phase and liquid electrolyte phase are summarized in Table I. The associated boundary conditions include constant charge-discharge rate, zero mass flux and heat convection on the electrodes surface, and continuity boundaries on the interface between electrodes and separator layer, which are similar to the settings of our previous impedance model.<sup>1</sup>

The impedance response of lithium-ion battery is typically obtained through an active interrogation process. Strictly following the same testing protocol of our experiments, the developed battery model was firstly used to simulate charge and discharge process, then a voltage perturbation is applied after each 10% depth of discharge (DOD) or depth of charge (DOC). The corresponding current output can be recorded through numerical analysis, and the simulated EIS response can be obtained according to the obtained model input and output signals: 15

$$\varphi(t) = \overline{\varphi} + \widetilde{\varphi} \exp(j\omega t)$$
 [3]

$$I(t) = \overline{I} + \widetilde{I} \exp[j(\omega t - \psi)]$$
 [4]

Table I. Governing equations.

#### Equation

Charge: 
$$\frac{\partial}{\partial x} \left( -\sigma_{j}^{eff} \frac{\partial \varphi_{1,j}}{\partial x} \right) = i_{j}^{tot}$$

$$\frac{\partial}{\partial x} \left( -\kappa_{j}^{eff} \frac{\partial \varphi_{2,j}}{\partial x} \right) + \frac{2RT(1-t_{+}^{0})}{F} \frac{\partial}{\partial x} \left( -\kappa_{j}^{eff} \frac{\partial (\ln c_{j})}{\partial x} \right) = i_{j}^{tot}$$

$$(2)$$

$$U_{j} = U_{j}^{ref} + (T - T_{ref}) \frac{\partial U_{j}}{\partial t};$$

$$(3)$$

$$\eta_{j} = \varphi_{1} - \varphi_{2} - U_{j} - \frac{i_{j}^{F}}{S_{j}} R_{f}; \eta_{s} = \varphi_{1} - \varphi_{2} - U_{s}^{ref}$$

$$\frac{\partial c_{j}^{s}}{\partial t} = D_{j}^{s} \frac{1}{r^{2}} \frac{\partial}{\partial r} \left( r^{2} \frac{\partial c_{j}^{s}}{\partial r} \right);$$

$$\varepsilon_{j} \frac{\partial c_{j}}{\partial t} = \frac{\partial}{\partial x} \left( D_{j}^{eff} \frac{\partial c_{j}}{\partial x} \right) + \frac{(1-t_{+}^{0})i_{j}^{tot}}{F}$$

$$D_{i}^{eff} = 10^{-8.43 - (54/(T - 229 - 0.0005c_{j})) - 0.00022c_{j}} \varepsilon_{j}^{brugg}$$

$$(5)$$

Heat: 
$$\rho c_p \frac{dT}{dt} = \lambda \frac{\partial^2 T}{\partial x^2} + Q_{rxn} + Q_{rev} + Q_{ohm}$$
 (7)

$$Q_{rxn} = i_j^F \left( \varphi_{1,j} - \varphi_{2,j} - U_j - \frac{i_j^F}{S_j} R_f \right); Q_{rev} = i_j^F T \frac{\partial U_j}{\partial T}, Q_{ohm} = \sigma_{eff} \left( \frac{\partial \varphi_1}{\partial x} \right)^2 + \kappa_{eff} \left( \frac{\partial \varphi_2}{\partial x} \right)^2 + \frac{2\kappa_{eff}RT}{F} (1 - t_+^0) \frac{\partial (\ln c)}{\partial x} \frac{\partial \varphi_2}{\partial x}$$
(8)

$$Z = Z_{re} + Z_{im} = \frac{\tilde{\varphi} \exp(j\omega t)}{\tilde{I} \exp(j(\omega t - \psi))} = \frac{\tilde{\varphi}}{\tilde{I}} \{\cos(\psi) + j \sin(\psi)\}$$
[5]

where,  $\overline{\phi}$  is the normal operating voltage;  $\widetilde{\phi}$  is the amplitude of the harmonic perturbation voltage; j is the square root of -1;  $\omega$  is the frequency;  $\widetilde{I}$  is the normal operating current;  $\widetilde{I}$  is the amplitude of current perturbation induced by the voltage perturbation;  $\psi$  is the phase shift of the harmonic current perturbation with respect to the harmonic voltage perturbation. Through this calculation procedure, the obtained simulated impedance spectra do not only involve the impact of battery material properties, operation conditions, but also involve the multi-transport processes and local charge variations during charge and discharge operation.

The mathematical model is numerically solved using the software package COMSOL Multiphysics V5.4. A classic pseudo 2D approach was used, <sup>17</sup> where a one-dimensional battery model and a two-dimensional electrode solid phase model. The battery charge or discharge operation from fully discharged state or fully charged state is firstly simulated at constate C-rate applied, which strictly followed our experimental procedure. Similarly, the EIS simulation then is carried out by applying a voltage perturbation of 5 mV in amplitude with frequency ranging from 10mHz to 10 kHz on the positive NMC electrode current collector surface, which also strictly followed the same protocols as our experimental EIS tests. The simulated impedance profile can be calculated based on the current output signal. The related model parameters have been listed in Table II.

#### **Results and Discussion**

Charge and discharge performance.—The measured voltage-capacity curves of the commercial cell at different C-rates are illustrated in Fig. 2. This is to demonstrate the rate capacity of this type of commercial cell and monitor the health of the cycled cylindrical cells before following impedance analysis. Two sets of experimental data, discharge curves and charge curves, are presented, which are obtained from two separate experiments: each discharge curve was obtained from fully charged state (100% SOC), while each charge curve was obtained from fully discharge state (0% SOC). It shows the capacity utilization of the cell decreases when the C-rate increases from 0.1C to 4C at discharge and when the C-rate increases from 0.1C to 1C at charge: on discharge, the capacity utilization at 0.1C is about 2500 mAh g<sup>-1</sup>, and it drops to 2250 mAh g<sup>-1</sup> and 1900 mAh g<sup>-1</sup> when the C-rate increases to 1C and 4C

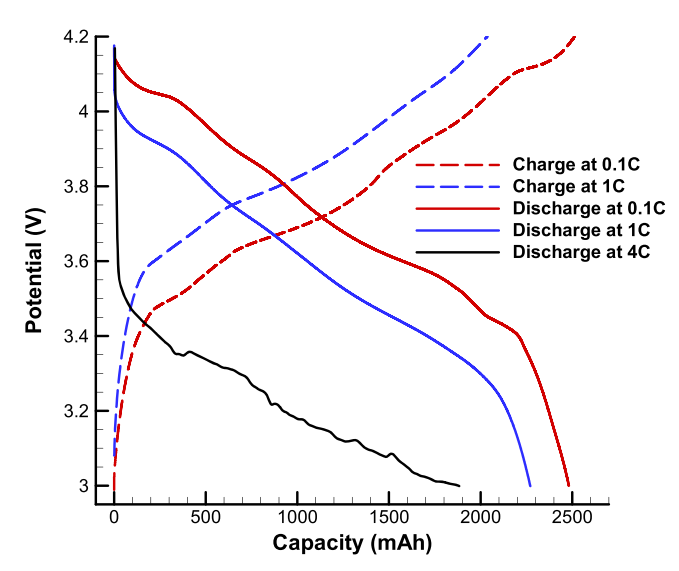


Figure 2. Charge and discharge behavior of the cell.

respectively. On charge, the capacity utilization is 2550 mAh g<sup>-1</sup> at 0.1C and decreases to 2200 mAh g<sup>-1</sup> at 1C. Clearly, the decrease of capacity utilization in the charge processes is slightly more sensitive to the C-rate rise comparing to discharge process. Besides, higher C-rate will lead to a higher cell voltage at the same remining capacity. These phenomena suggest that battery internal processes could significantly influence the voltage behavior of this NCA commercial cell, and its performance varies with cell operating conditions. To explore the behavior of this cylindrical cell at different SOC states, a series of EIS experiments were design and conducted in the following sections.

**Different SOC conditions.**—The state of charge reflects the amount of charge carriers, Li-ions, stored in two cell electrodes. Figure 3 illustrates the impedance of the cylindrical cell measured at different C-rates in both discharge and charge processes. As described in the experimental section, two separate EIS experiments were conducted in discharge and charge respectively: the impedance data was recorded at different SOC states in the discharge process, then the impedance was collected at different SOCs in the charge process, while a long relaxation period (2 h) was applied before each EIS test. As can be seen, the impedance profiles of this commercial cylindrical cell contain arc(s) at high-middle frequency range, while

Table	II.	Model	parameters.
-------	-----	-------	-------------

	Anode	Cathode
Active material	Graphite	NCA
Electrode thickness:	$1.2 \times 10^{-4}$ m	$1.2 \times 10^{-4}$ m
Particle size (radius)	$1.25 \times 10^{-5}$ m	$5 \times 10^{-6} \text{m}$
Li diffusivity:	$3.9 \times 10^{-14} \text{m}^2 \text{s}^{-1}$	$1.2 \times 10^{-13} \text{m}^2 \text{s}^{-1}$
Exchange current density:	$2 \times 10^{1*} \text{A m}^{-2}$	$5 \times 10^{1*} \text{A m}^{-2}$
Electrical double layer capacity:	$0.35^*F$	$0.3^*F$
Electrical conductivity:	$100 \ \mathrm{S \ m}^{-1}$	$4 \mathrm{Sm}^{-1}$
Volume fraction of solid phase:	0.3	0.47
Separator thickness:	$2 \times 10^{-5}$ m	
Electrolyte salt diffusivity:	$7.5 \times 10^{-11} \text{m}^2 \text{s}^{-1}$	
Cationic transport number:	0.37	
Max solid phase concentration:	$27,000 \text{ mol m}^{-3}$	
Initial passive film resistance:	$1 \times 10^{-2} \cdot \Omega \text{m}^{-2}$	
Contact resistance parameter (a, b):	$2 \times 10^{-3}, 1 \times 10^{-3*}$	
Initial electrolyte salt concentration:	$1 \times 10^3 \text{mol m}^{-3}$	
Bruggeman coefficient:	1.5	
*	(Adjusted/Assumed value)	

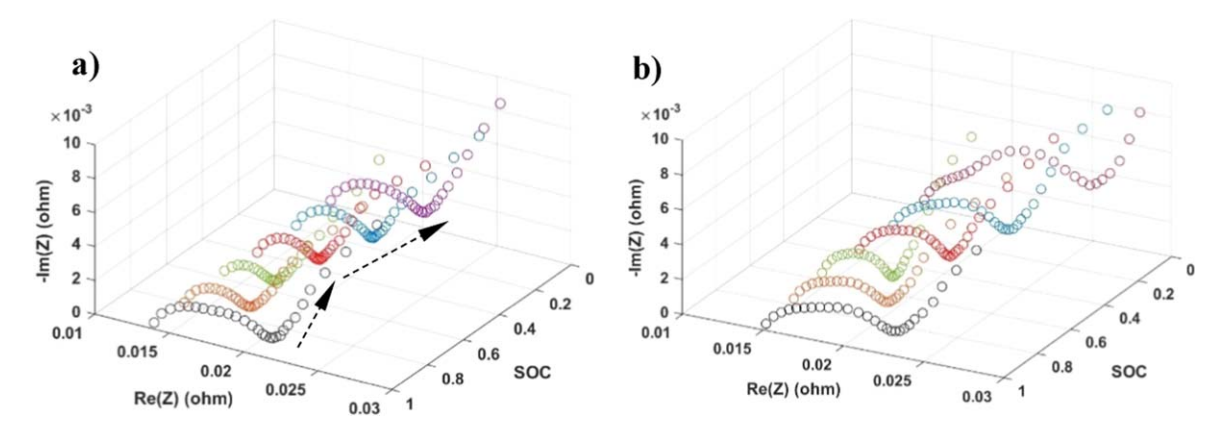


Figure 3. Impedance response of the cylindrical cell at different SOC conditions during: (a) discharge process at 0.1C; (b) charge process at 0.1C.

a pure capacitive behavior can be seen in the low frequency section. In the discharge (Fig. 3a), it is interesting to see that: the high-middle frequency arc of the impedance profile decreases its size at first when the SOC of battery decreases from 100% to around 60%. When the cell is further discharged from 60% SOC to 0% SOC, the size of the high-middle frequency arc increases its size back. Meanwhile, the low-frequency branch of the impedance profile does not show any change in different SOCs. Similarly, such a "SOC dependent" behavior of impedance can also be observed in the EIS tests during charge process (in Fig. 3b). As known, the charge and mass transport process are typically represented by the high-mid frequency arcs on impedance curve, while low frequency branch stands for the solid-state diffusion process. 18,19 These observations suggest the cell internal resistance and capacitance are influenced by the state of charge, and cell performance will vary with different SOC conditions.

Different C-rates.—Figure 4 shows the impedance profiles of the cylindrical cell during the discharge process when the discharge C-rate is set at 1C and 4C respectively. The obtained impedance curves show that the high-mid frequency arc of the impedance decreases its size first and then increase as the SOC drops from 100% to 0% in both 1C and 4C experiments. Although the magnitude of the changes is slightly different, the "SOC dependent" impedance exists in all tested C-rates. Besides, we also found this SOC dependent impedance behavior is reproduceable by repeating the EIS tests at different C-rates three times on six cells. Since the charge-discharge rates represent the flux of lithium ions moving between two electrodes and reflect the intensity of mass transport inside battery cell, these observations imply that the mass transport should not be the primary reason leading to the SOC dependent behavior of the cell impedance response.

Temperature impact.—To explore the impact of operation temperature on the cylindrical battery behavior and impedance, we conducted the same EIS tests (same testing protocol) at 0.1C and 1C, respectively, under different SOCs at a low temperature condition, 10 °C. As illustrated in Fig. 5, the obtained impedance curves at 10 °C (both 0.1C and 1C) are slightly larger than these of 25 °C in magnitude. This is because a low operation temperature could significantly reduce the intensity of both charge and mass transport process inside cell and also influence the solid-state diffusion process. However, at 10 °C, it is interesting that cell impedance curves still have the SOC dependent behavior even though it is not as obvious as that under 25 °C condition. These observations suggest that operating temperature could influence the significance of the SOC dependent impedance behavior of this type of commercial cell but should not be the main cause of this phenomenon.

Modeling analysis.-Modeling is always an important tool to assist in understanding the mechanism behind experimental observations. As described in above modeling section, an impedance model was developed to reproduce the experimental procedure and analyze the experimental observations. Figure 6 illustrates the modeled impedance profiles of the cell at different SOC conditions when the operation temperatures were set at 25 °C and 10 °C respectively. It shows that the impedance arcs in the high-middle frequency range at 10 °C are larger than that at 25 °C. This is because the modeled transport processes are all temperature dependent, and a higher temperature could directly lead to a different parameter value (e.g., charge conductivity, diffusion coefficient, etc). These results are consistent with our above experimental data. Meanwhile, it is obvious that the impedance profiles are nearly the same (overlapped) under the same operation temperature. Besides, we also simulated the influence of charge-discharge C-rate in Fig. 7, in which a

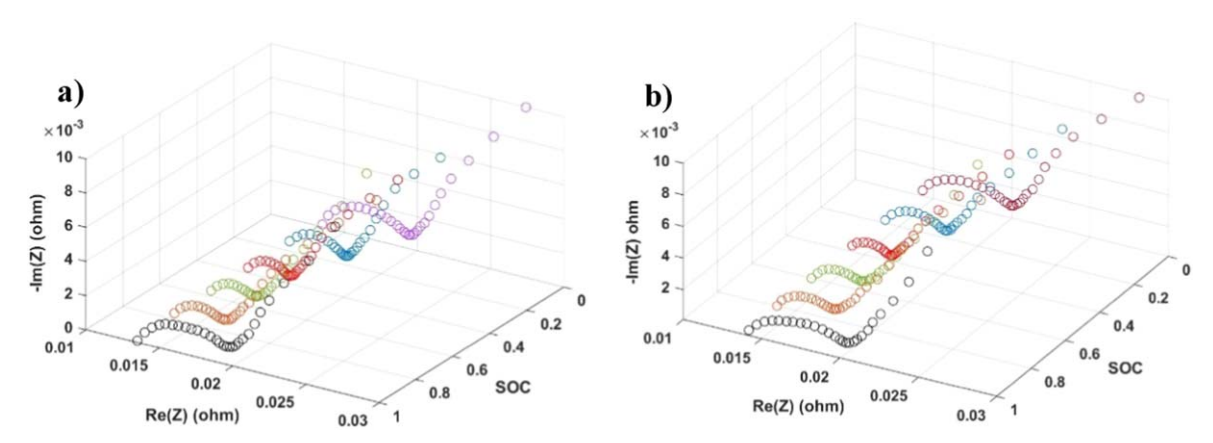


**Figure 4.** Impedance response of the cylindrical cell at different SOC conditions when the operating temperature is 25 °C and charge-discharge C rate is: (a) 1C; (b) 4C.

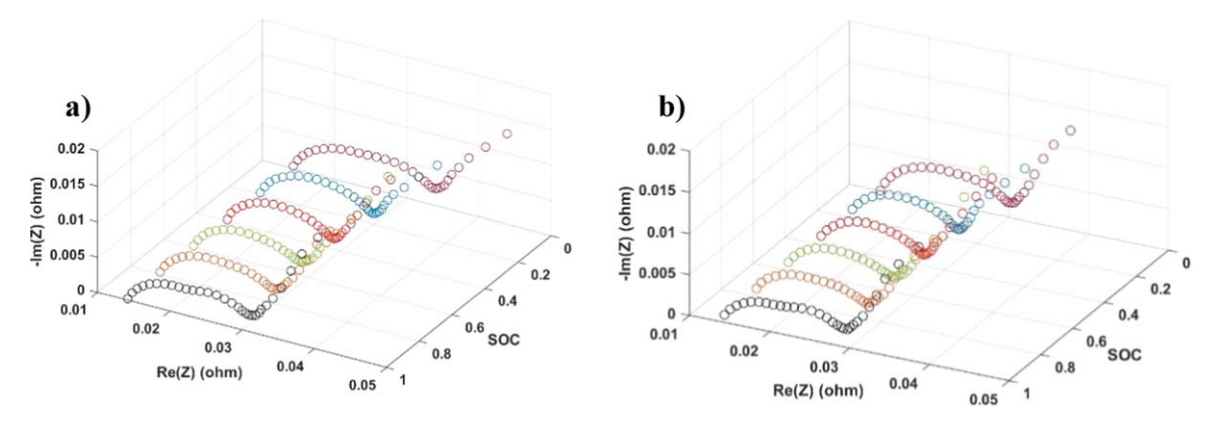
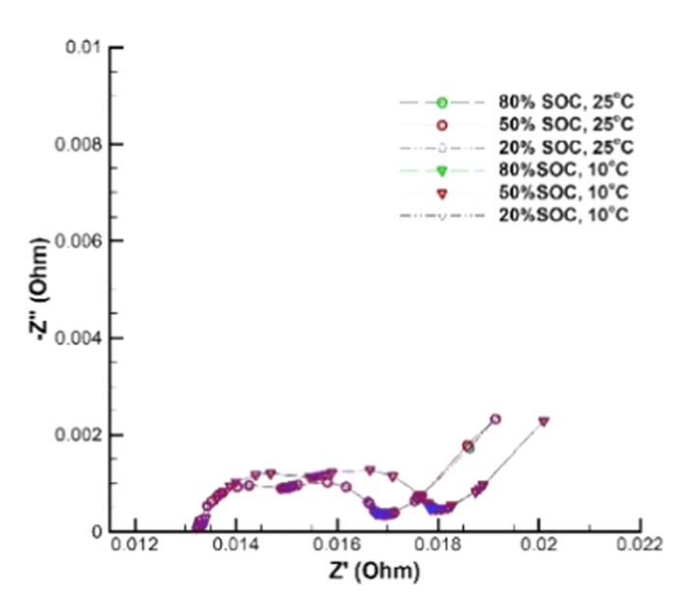
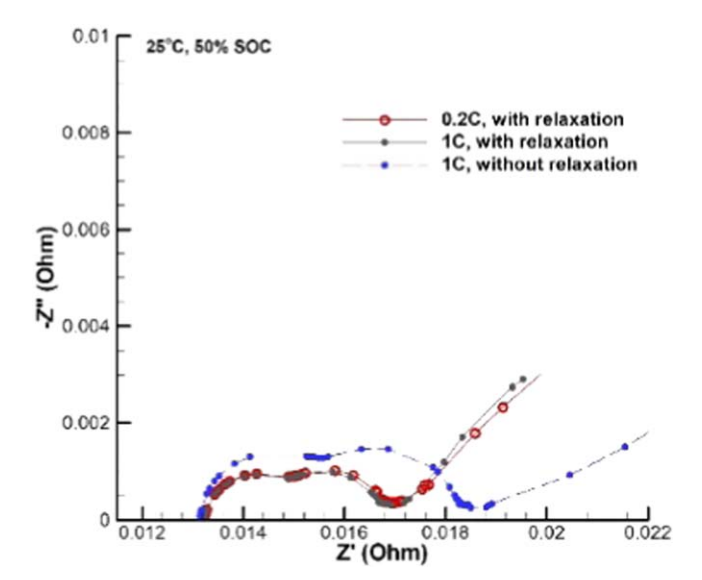


Figure 5. Impact of low operating temperature, 10 °C, on the impedance response of the cylindrical cell at different SOC conditions: (a) 0.1C; (b) 1C.



**Figure 6.** Modeled the impedance response of the cylindrical cell at different SOC conditions and different operating temperature.



**Figure 7.** Influence of charge-discharge rate and the relaxation impact on the modeled impedance response.

relaxation period was simulated by temporarily removing the charge-discharge operation. As shown, without relaxation, the

impedance profile of 0.2C at 50%SOC has a smaller high-middle frequency arc than that of 1C at 50%SOC. However, when a 2-h relaxation was applied (before the EIS test), two impedance profiles are overlapped. These interesting results indicate that the operating temperature and charge-discharge rate could significantly influence the impedance response of the battery but should not directly cause the variation of the impedance response at different SOC conditions.

As known, the intercalation and deintercalation of lithium ions could inevitably lead to the expansion and contraction of electrode active materials. Since the state of charge of a battery cell represents the amount of stored lithium, the contact resistance between the active material particles and the conductive matrix could vary with SOC state. Hence, to further explore the potential reasons leading to above SOC dependent impedance response, a particle-conductive contact resistance,  $R_{cr}$ , was introduced into the developed model. Since the contact resistance of this commercial cell is unknown (data is not available), we assumed a linear relationship between contact resistance and lithium concentration to capture and simplify the expansion or contraction of electrodes during the intercalation or deintercalation of lithium in the modeling, where the variation of capacitance was neglected:

$$R_f = R_{f,SEI} + R_{cr,j}; R_{cr,j} = a \cdot c_{Li,j} + b, j = neg, pos$$
 [6]

where, *a* and *b* are constants. Modeling results are shown in Fig. 8, in which the modeled impedance response varies with SOC: the size of high-middle frequency arc decreases when SOC changes from 20% to 50% then increases when SOC changes from 50% to 80%. This successfully reproduced the SOC dependent impedance response observed in our above experiments. These results demonstrate the contact resistance is one of the factors that could lead to the observed SOC dependent impedance. Meanwhile, modeling results also suggest that if the expansion and contraction of commercial cell electrodes were not well controlled in charge or discharge, cell performance will have a clear variation at different SOC conditions and will directly influence cell output performance during both charge and discharge.

#### Conclusions

In this study, a series of EIS experiment was carried out to explore the behavior of a commercial cylindrical cell at different SOC conditions. We found this type of commercial cell had a SOC dependent impedance response. After conducting impedance test at different operating conditions, experimental results showed that such SOC dependent impedance behavior existed in different temperatures and C-rates, which suggests the mass transport should not be the primary reason leading to this phenomenon. To explore the potential reasons and mechanisms behind experimental observations, an impedance model was developed to simulate battery impedance responses. Modeling results showed that the operating temperature and charge-discharge rate could significantly influence the

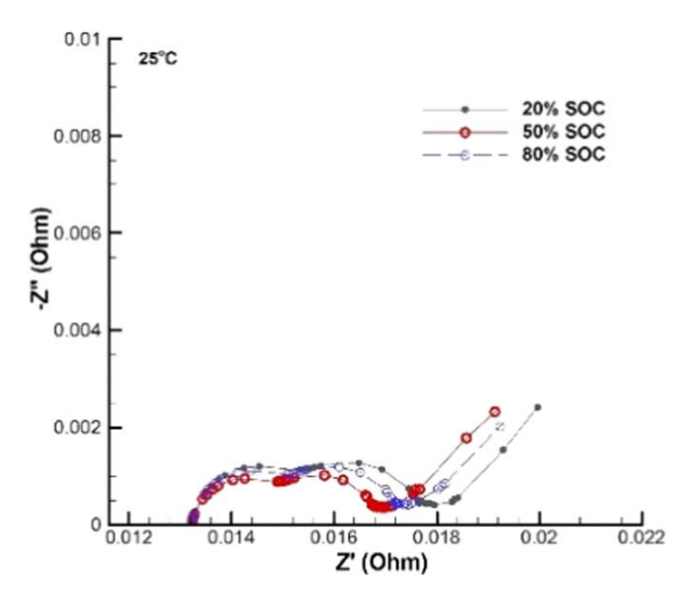


**Figure 8.** The impact of contact resistance on the modeled cell impedance response at different SOC conditions.

impedance response of the battery but could not directly cause the variation of the impedance response at different SOC conditions. By considering the contact resistance between the active material particles and the conductive matrix, which could vary with SOC state due to the inevitable expansion and contraction of electrode active materials, we found contact resistance could lead to a SOC dependent impedance behavior of the commercial cell. These results also indicate the expansion and contraction of commercial cell electrodes during charge and discharge have a direct influence on the battery output performance.

# Acknowledgments

The authors gratefully acknowledge the support from the Korea Electric Power Corporation (R21XO01-3) and the financial support from National Science Foundation (NSF U.S. Grant No. 1816197).

#### **ORCID**

Yuanyuan Xie https://orcid.org/0000-0002-9859-1149

#### References

- P. Berg, M. Spielbauer, M. Tillinger, M. Merkel, M. Schoenfuss, O. Bohlen, and A. Jossen, *Journal of Energy Storage*, 31, 101499 (2020).
- 2. S. Baksa and W. Yourey, Batteries, 4, 45 (2018).
- S. Panchal, M. Mathew, R. Fraser, and M. Fowler, *Appl. Therm. Eng.*, 135, 123 (2018).
- 4. S. Al-Hallaj and J. R. Selman, J. Power Sources, 110, 341 (2002).
- 5. U. Tröltzsch, O. Kanoun, and H.-R. Tränkler, *Electrochim. Acta*, 51, 1664 (2006).
- 6. F. La Mantia, J. Vetter, and P. Novák, *Electrochim. Acta*, 53, 4109 (2008).
- J. Illig, J. P. Schmidt, M. Weiss, A. Weber, and E. Ivers-Tiffée, J. Power Sources, 239, 670 (2013).
- M. Spielbauer, P. Berg, M. Ringat, O. Bohlen, and A. Jossen, *Journal of Energy Storage*, 26, 101039 (2019).
- K. Amine, C. Chen, J. Liu, M. Hammond, A. Jansen, D. Dees, I. Bloom, D. Vissers, and G. Henriksen, *J. Power Sources*, 97, 684 (2001).
- M. Balasundaram, V. Ramar, C. Yap, L. Li, A. A. Tay, and P. Balaya, *J. Power Sources*, 328, 413 (2016).
- T. Momma, M. Matsunaga, D. Mukoyama, and T. Osaka, J. Power Sources, 216, 304 (2012).
- D. Andre, M. Meiler, K. Steiner, C. Wimmer, T. Soczka-Guth, and D. Sauer, J. Power Sources, 196, 5334 (2011).
- D. Andre, M. Meiler, K. Steiner, H. Walz, T. Soczka-Guth, and D. Sauer, J. Power Sources, 196, 5349 (2011).
- V. Ramadesigan, P. W. Northrop, S. De, S. Santhanagopalan, R. D. Braatz, and V. R. Subramanian, J. Electrochem. Soc., 159, R31 (2012).
- 15. Y. Xie, J. Li, and C. Yuan, *Electrochim. Acta*, 127, 266 (2014).
- J. B. Quinn, T. Waldmann, K. Richter, M. Kasper, and M. Wohlfahrt-Mehrens, J. Electrochem. Soc., 165, A3284 (2018).
- 17. L. Cai and R. E. White, J. Power Sources, 196, 5985 (2011).
- J. P. Schmidt, T. Chrobak, M. Ender, J. Illig, D. Klotz, and E. Ivers-Tiffée, J. Power Sources, 196, 5342 (2011).
- J. P. Schmidt, P. Berg, M. Schönleber, A. Weber, and E. Ivers-Tiffée, J. Power Sources, 221, 70 (2013).
- A. Pfrang, A. Kersys, A. Kriston, D. Sauer, C. Rahe, S. Käbitz, and E. Figgemeier, J. Power Sources, 392, 168 (2018).
- P. Albertus, J. Christensen, and J. Newman, J. Electrochem. Soc., 156, A606 (2009).